Preparation and photocatalytic "memory" effect of Cu-Cu$_2$O/SnO$_2$ composite

Yawei Hu[a,b,*], Yan Zhang[a], Hui Gao[a], Tong Fang[a], Xin Du[a], Ning Zhao[a,b]

[a]*College of Chemistry and Chemical Engineering, Shaanxi University of Science and Technology, Xi'an, Shaanxi 710021, China,
Tel.: +86 29 86168830; emails: huyawei@sust.edu.cn (Y. Hu), 1789501348@qq.com (Y. Zhang), 2692767348@qq.com (H. Gao),
940519636@qq.com (T. Fang), 643544886@qq.com (X. Du), zhaoning@sust.edu.cn (N. Zhao)*
[b]*Key Laboratory of Chemical Additives for China National Light Industry, Xi'an, Shaanxi 710021, China*

ABSTRACT

The photocatalyst with photocatalytic "memory" effect can solve the inherent activity loss of traditional photocatalysts when the light is turned off, which would greatly improve its catalytic efficiency in the field of wastewater treatment. In this work, Cu-Cu$_2$O/SnO$_2$ composites with different SnO$_2$ contents were prepared by adding different amounts of SnO$_2$ colloidal solution to Cu-Cu$_2$O suspension *via* a solvothermal method. The product was characterized by X-ray diffraction, scanning electron microscopy, transmission electron microscopy, UV-Vis diffuse reflectance spectroscopy, X-ray photoelectron spectroscopy, zeta potential, transient photocurrent response and electrochemical impedance spectroscopy. The photocatalytic activity and "memory" effect of Cu-Cu$_2$O/ SnO$_2$ composite were investigated through methyl orange (MO) solution degradation experiments. The results show that the Cu-Cu$_2$O/SnO$_2$ of Sn0.75 sample possesses the best photocatalytic performance and the degradation rate of MO is 93.7% under visible light for 120 min. Furthermore, the removal rate of methyl orange solution is increased by 17.2% in dark for 3 h after the Sn0.75 photocatalyst is illuminated for 1 h, which displays that the Cu-Cu$_2$O/SnO$_2$ photocatalyst possesses the post-illumination "memory" activity. This work will provide an experimental basis for highly efficient round-the-clock photocatalysts.

Keywords: Cuprous oxide; Stannic oxide; Photocatalytic "memory" effect; Energy storage/release

1. Introduction

For decades, environmental pollution caused by urbanization and industrialization has become an increasingly serious problem, especially inorganic and organic pollutants in wastewater which are usually difficult to be removed and seriously affect human health [1–3]. Although conventional methods such as ozonation, photo-Fenton processes, adsorption, ion exchange and advanced oxidation processes have been widely used in wastewater treatment, organic matter is difficult to be completely eliminated and may cause secondary pollution [4–6]. Therefore, finding more efficient removal methods is the pursuit of researchers. It is well known that the surface of the catalyst has enough adsorption sites which is very beneficial to enhancing its photocatalytic effect [7,8]. This is due to the fact that free radicals are quenched by pollutants in water and photocatalysis occurs on the catalyst surface, in which adsorption is very important to promote the concentrate of pollutant on the catalytic surface to enhance the photocatalytic efficiency. Cuprous oxide (Cu$_2$O), as a metal oxide semiconductor catalyst with excellent band gap, has been widely used in photocatalytic fields for wastewater treatment [9–11]. However, the photocatalytic efficiency of Cu$_2$O is not as high as expected due to the rapid recombination of light-induced electron–hole pairs [12–14]. Therefore, efforts have been made to combine Cu$_2$O with other semiconductor, metal or organic carbon materials to

* Corresponding author.

decrease the combination of electrons and holes in order to improve the photocatalytic activity of Cu_2O [15–18].

However, most photocatalysts rapidly lost their catalytic activities when the illumination is switched off. Therefore, it is very promising to explore the photocatalysts which would still remain catalytic activity in dark. Several photocatalysts with an interesting post-illumination "memory" effect had been reported, which could still maintain catalytic activity in dark after the illumination is switched off [19–22]. These photocatalysts contain both the light-absorbing component and the electron-storing component. The electron-storing component can store photo-generated carriers from photocatalysts under light irradiations and release these carriers when the illumination is switched off [23]. Till now, several materials have been found to have photocatalytic "memory" effect, such as Bi_2WO_6 [24] and Au@Cu_2O [25]. In this work, we obtained Cu-Cu_2O/SnO_2 composite photocatalysts with the post-illumination "memory" activity *via* a solvothermal method.

2. Materials and methods

2.1. Materials

All reagents are analytical grade and no further purification is required in this work.

2.2. Preparation of sample

2.2.1. Synthesis of Cu-Cu_2O particles

4.5 mmol $Cu(NO_3)_2$ was completely dissolved in a mixture with 7 mL glycerol, 7 mL ethanol and 10 mL water. Then 9 mmol urea was added into the above solution and dissolved completely, followed by transferring to a Teflon-lined stainless-steel autoclave and heating at 170°C for 9 h. After the reaction and cooling to room temperature, the product was collected, washed, and dried in a 60°C vacuum oven for 12 h. The sample obtained is named Base.

2.2.2. Synthesis of Cu-Cu_2O/SnO_2 composites

A serial of Cu-Cu_2O/SnO_2 composites were prepared through solvothermal method using Cu-Cu_2O particles of Base and a small amount of SnO_2 colloidal solution as precursors. Firstly, the colloidal SnO_2 solution was prepared at room temperature by adding 0.335 g of thiourea and 1.015 g $SnCl_2·2H_2O$ in 30 mL deionized water with continuously magnetically stirring for 40 h in air. Then a small amount of SnO_2 colloidal solution was slowly dropped in Cu-Cu_2O suspension containing 36 mg Base sample and 18 mL H_2O with contentiously stirring for 1 h. Finally, the mixture was transferred into a Teflon-lined stainless-steel autoclave and heated at 170°C for 6 h. After cooling to room temperature, the products were collected, washed, and dried in a 60°C vacuum oven for 12 h. The obtained samples were named Sn0, Sn0.05, Sn0.25, Sn0.5, Sn0.75, Sn1.0 and Sn5.0, respectively, when the volumes of SnO_2 colloidal solution added into the Base sample were 0, 0.05, 0.25, 0.5, 0.75, 1.0 and 5.0 mL.

2.3. Characterization

An X-ray powder diffractometer (XRD, Rigaku-Ultima IV, Japan) was used to characterize the phase of the sample with Cu-Kα radiation ($λ = 0.15405$ nm) at a scanning speed of 8°/min^{-1} ranging from 20° to 80°. A scanning electron microscopy (SEM, FEI Verios 460, America) and a high-resolution transmission electron microscopy (HR-TEM, Tecnai G2 F20 S-TWIN, America) were used to observe the morphology and crystal lattice. The UV-Vis absorption spectra of the samples were acquired by a UV-Vis diffuse reflection spectrometer (UV-Vis DRS, Lambda 950, PerkinElmer, America) using $BaSO_4$ as a reference. The surface composition was obtained with an X-ray photoelectron spectroscopy (XPS, AXIS Supra, Kratos, UK). Transient photocurrent response and electrochemical impedance spectroscopy (EIS) were recorded on a electrochemical workstation (CHI660E, Shanghai, China) in the presence of 0.5 $mol·L^{-1}$ sodium sulfite as an electrolyte, Ag/AgCl as the reference electrode, carbon rod as the counter, and the Cu-Cu_2O or Cu-Cu_2O/SnO_2 electrode prepared as the working electrode. Cu-Cu_2O and Cu-Cu_2O/SnO_2 electrodes were prepared as follows: 5 mg sample, 1 mg carbon black, 1 mL ethanol and 0.5 mL 5% nafion dispersion were added into a centrifuge tube, respectively. After sealing the centrifuge tube, the dispersion was evenly proceeded by an ultrasonic cleaner for 20 min, then the 20–30 μL dispersed solution was dropped onto the glass carbon electrode until the sample was evenly dispersed on the electrode surface after 2–3 times. Zeta potential was recorded on a Zetasizer Nano ZS (Malvern, UK) to obtain the point of zero charge. And the photodegradation of methyl orange (MO) solution was used to evaluate the photocatalytic activity of the Cu-Cu_2O/SnO_2 composite by measuring the absorption intensity at 462 nm with a visible spectrophotometer (723N, Shanghai, China), in which a 500 W xenon lamp with a UV filter ($λ > 420$ nm) was assembled in a visible photoreactor.

In this paper, all the photocatalytic degradation experiments were carried out in neutral aqueous solution except the effect of pH on the photocatalytic degradation performance. 10 mg sample was put into a 50 mL MO solution (20 $mg·L^{-1}$, pH = 7), followed by magnetically stirring in dark for 30 min. Then a 5 mL MO solution was taken out after every 30 min visible light irradiation, and its absorption intensity at 462 nm was recorded after centrifuged. In the active species trapping experiment, 1 mM benzoquinone (BQ), isopropanol (IPA) and ammonium oxalate (AO) were applied as scavenging agents of superoxide radical ($^•O_2^-$), hydroxyl radical ($^•OH$), photogenerated positively charged hole (h^+), respectively [26,27]. Other experimental conditions were identical as those mentioned in the above photodegradation experiment.

To investigate photocatalytic "memory" activity, a 10 mg Cu-Cu_2O/SnO_2 composite was firstly irradiated under the xenon lamp for 1 h. Then, the lamp was shut off and the degradation experiment was carried out in dark over the pre-illuminated samples. Other experimental conditions and processes were the same as the photocatalytic degradation experiment.

3. Results and discussion

3.1. Crystalline and phase structure characterizations

Fig. 1 shows the X-ray diffraction (XRD) patterns of the Base sample and Cu-Cu_2O/SnO_2 composites with different loads of SnO_2. It could be observed that the Base and Sn0

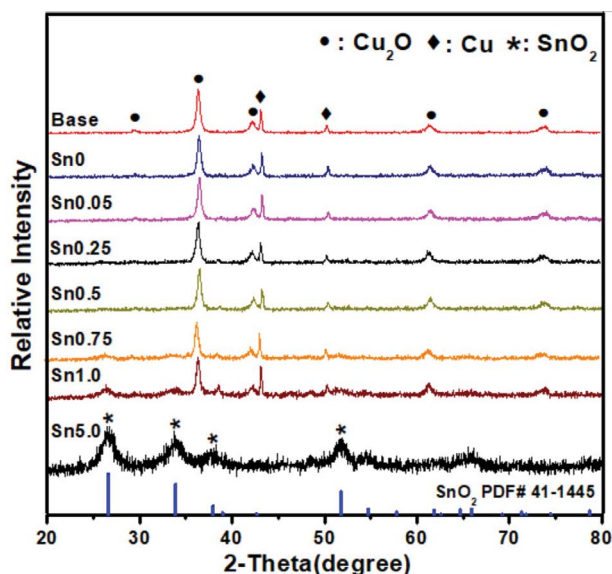Fig. 1. X-ray diffraction patterns of base sample and Cu-Cu$_2$O/SnO$_2$ composites with different SnO$_2$ loading.

appear similar diffraction peaks which displays the second solvothermal treatment nearly has no influence on the phase of the Base sample. And they both exhibit two sets of XRD peaks of Cu$_2$O and Cu. The peaks at 29.6°, 36.4°, 42.3°, 61.3° and 73.5° are consistent with the diffraction peaks of cuprite Cu$_2$O standard card (PDF card No. 05-0667). While other peaks could be attributed to Cu in agreement with the standard card (PDF card No. 65-9026), indicating the coexistence of Cu$_2$O and Cu. Furthermore, the diffraction peaks of SnO$_2$ appear and the peak intensities of SnO$_2$ enhance with the increase of the amount of the SnO$_2$ colloidal solution added, which show the amount of SnO$_2$ in the Cu-Cu$_2$O is increasing. However, there is no obvious peak in the sample Sn0.05, which might be due to the very small amount of SnO$_2$ loading. And the peaks of Cu$_2$O and Cu nearly could not be observed in the pattern of Sn5.0, which might be attributed to the large SnO$_2$ loading.

3.2. Morphological observation

The morphologies of the samples were investigated by SEM and transmission electron microscopy. From Fig. 2a and b, the samples of Base and Sn0 are both solid spheres. However, the average size of Sn0 is smaller and its surface is rougher than that of the Base sample. After SnO$_2$ added, the sphere surfaces are loose and porous (Fig. 2c–g), and the Cu-Cu$_2$O/SnO$_2$ core-shell structure forms (insert of Fig. 2e). The surface of Sn5.0 (Fig. 2g) is unregular and loose, which might be due to formation of the amount of SnO$_2$. The HR-TEM image of Sn0.75 (Fig. 2h) was characterized. The measured crystal face distance of 0.34 nm matches with the (101) crystal plane of SnO$_2$, and the crystal face distances of 0.24 and 0.20 nm are corresponding to the crystal plane of Cu$_2$O (111) and Cu (111), respectively. Moreover, the heterogeneous structure of SnO$_2$-Cu$_2$O could be observed clearly, which would enhance photoelectron transport and photocatalytic activity [28].

3.3. Chemical state test

The XPS survey spectrum of sample Sn0.75 (Fig. 3a) shows the peaks of Sn and Cu elements. Fig. 3b shows the high resolution XPS spectral peak of Sn 3d$_{5/2}$. Sn^{4+} 3d$_{5/2}$ and Sn^{2+} 3d$_{5/2}$ peaks fit well at 486.6 and 485.6 eV, respectively. It has been reported that Sn^{2+} can be detected on the surface of SnO$_2$ nanoparticles because the Sn^{2+} state can be produced by trapping electrons in tin oxide [29–31]. Herein, Sn^{4+} traps the electrons from Cu$_2$O and turns into Sn^{2+}.

3.4. UV-Vis absorption spectra analysis

The UV-Vis DRS spectra of the samples are shown in Fig. 4. The result shows that the samples have good absorption ability in the range of visible wavelength, and the absorption edges are red shifted except for Sn5.0, which may be related to the SnO$_2$ loading in Cu-Cu$_2$O. Moreover, the absorption intensity increases with the SnO$_2$ loading content. Sn0.75 shows the strongest light absorption. And the light absorption intensity decreases with the further load of SnO$_2$. The increase of absorption intensity and red-shift absorption edge might lead to enhanced photocatalytic activity.

3.5. Photodegradation of pollutants on Cu$_2$O/SnO$_2$

The concentration of MO solution within 120 min was monitored under visible light to determine the photocatalytic activity (Fig. 5). Degradation efficiency is defined as $1-C_t/C_0$, where C_0 and C_t are the initial concentration of MO solution and that of the reaction process, respectively. As can be seen from Fig. 5a, the degradation efficiency of MO is only about 1.2% in the absence of any photocatalyst under visible light illumination for 120 min. And the degradation efficiency of MO is 15.4% using the Base as a photocatalyst. However, the degradation efficiency of methyl orange with Sn0 photocatalyst, which was prepared via the solvothermal method with the sample of Base as precursor, is up to 27.6%. The reason might be attributed to the loose surface morphology and small particle size which are caused by the second solvothermal process. Moreover, with the SnO$_2$ added, the degradation efficiency of MO increases and achieves its highest when the photocatalyst is Sn0.75. The reason might to be that the addition of SnO$_2$ could effectively reduce the photogenic hole and electron recombination [32], which would improve the photocatalytic performance. However, when SnO$_2$ is further added, the degradation efficiency of MO decreases. The reason might be the excess SnO$_2$ would cover the active sites of the photocatalyst and lead to a decrease of photocatalytic activity.

Degradation of MO solution is regarded as a first-order linear reaction, and the reaction equation:

$$-K_t = \ln\left(\frac{C_t}{C_0}\right)$$

where t is the photocatalytic reaction time, and K is the corresponding degradation rate constant. Fig. 5b shows the linear relationship between t and $\ln(C_t/C_0)$ of MO photodegradation by different catalysts, where the slope is
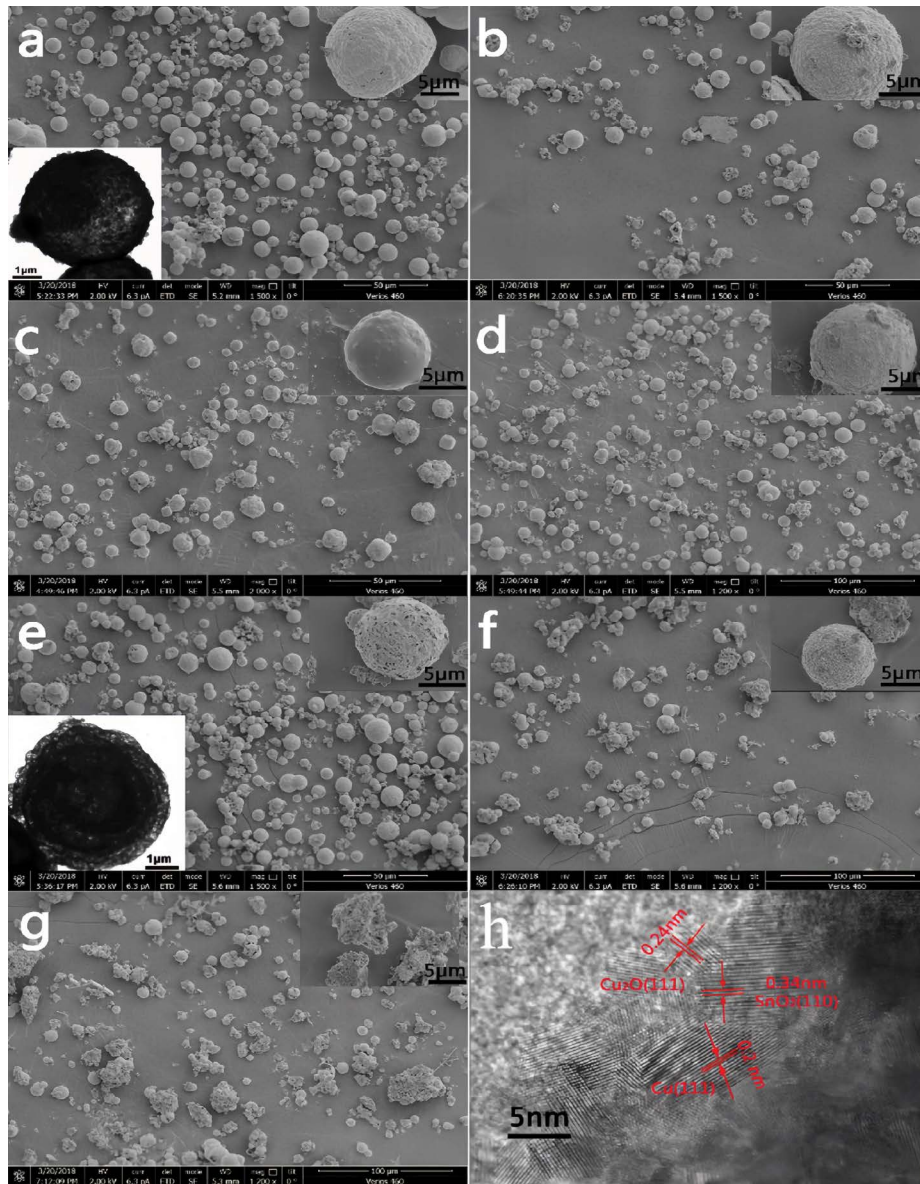
Fig. 2. Scanning electron microscopy and transmission electron microscopy images of the samples, (a) base of Cu-Cu$_2$O, (b–g) Sn0, Sn0.05, Sn0.25, Sn0.75, Sn1.0 and Sn5.0, and (h) high-resolution transmission electron microscopy image of Sn0.75.
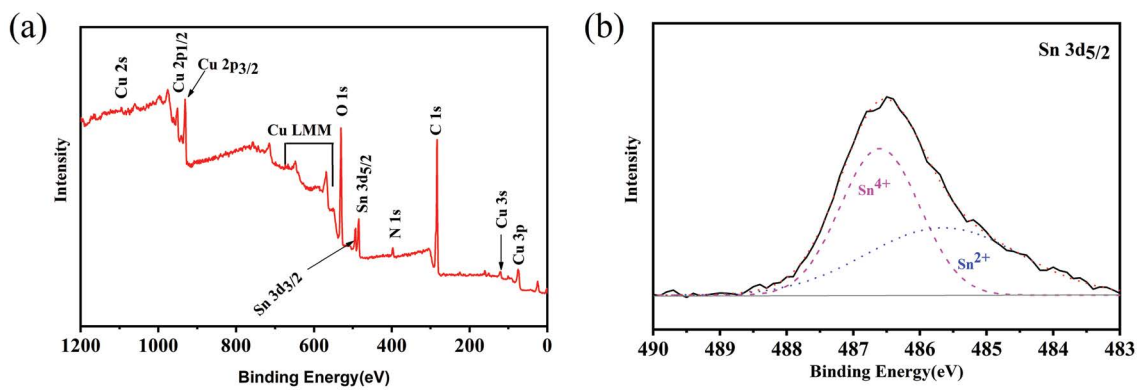

Fig. 3. X-ray photoelectron spectra of Sn0.75, (a) survey spectrum and (b) high-resolution spectrum over Sn 3d$_{5/2}$ peak.

the photodegradation rate constant K. The photocatalytic degradation rate constant K value of Sn0.75 for MO solution is 0.02123 min^{-1}, which is 14.7 times of that of Sn0 (0.00144 min^{-1}). Therefore, the photocatalytic property of Cu-Cu$_2$O is greatly improved after SnO$_2$ loaded. The effect of pH on photocatalytic degradation (Fig. 5c) shows that Sn0.75 has good photocatalytic activity in weak acid or neutral solution, and its photocatalytic degradation performance reduces distinctly in strong acid and alkaline environment. Fig. 5d shows the photocatalytic stability of Sn0.75 which was evaluated by repeating the MO degradation experiment. The experimental results show that the degradation rate of Sn0.75 still reaches 79.0% after four cycles of experiment, indicating Sn0.75 has good photocatalytic stability.

In order to explore the universality of Sn0.75 to degrade organic pollutants, the tetracycline degradation was proceeded, and the results are shown in Fig. 5e and f. It can be seen that the degradation efficiency of Sn0.75 for tetracycline is higher than that of Sn0 after 120 min illumination, and the photocatalytic degradation rate constant K value of Sn0.75 for tetracycline is 1.5 times of that of Sn0. Therefore, Sn0.75 can degrade a variety of pollutants and has universal applicability.

Zeta potential was measured as a function of the pH of the suspension, as shown in Fig. 6. The zeta potential of Sn0.75 decreases with pH value increasing. The point of zero charge (pzc) of Sn0.75 is 7.3 which implies that the fabricated Sn0.75 is positively charged at pH below pzc and
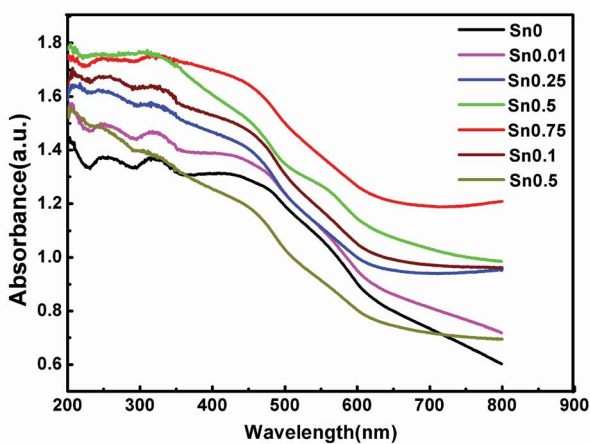

Fig. 4. UV-Vis diffuse reflectance spectroscopy spectra of Cu-Cu$_2$O/SnO$_2$ composite.
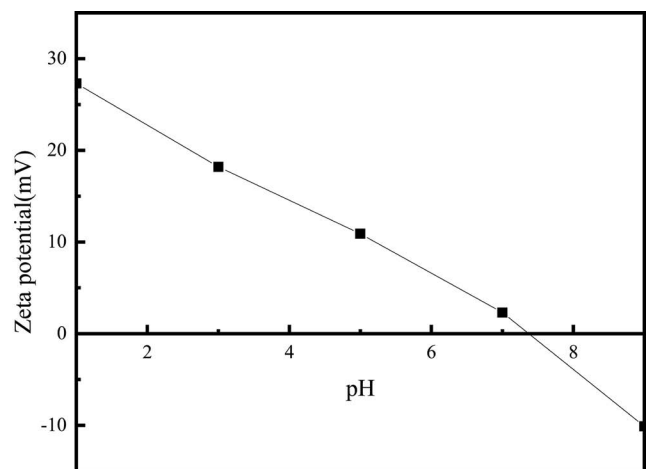

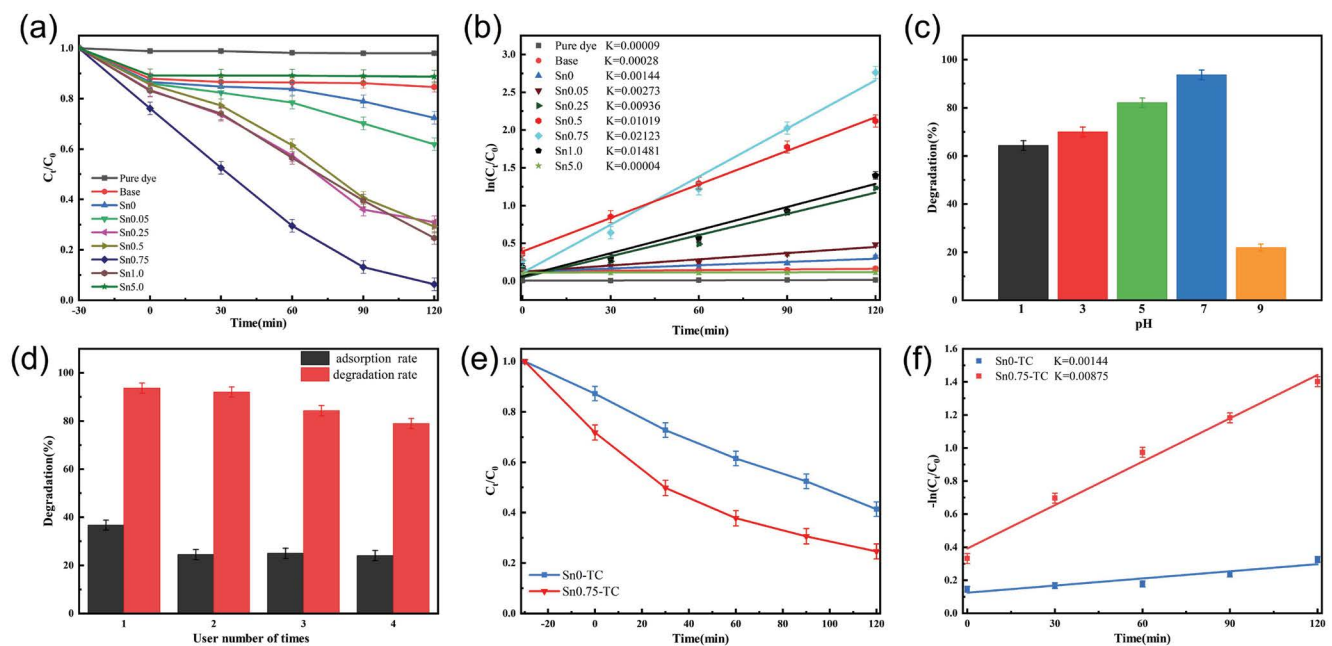Fig. 6. Zeta potential measurement of Sn0.75 in different pH.

Fig. 5. (a,b) Photocatalytic degradation of methyl orange solution and kinetic characteristic under different catalysts, (c) effect of pH on photocatalytic degradation methyl orange, (d) cyclic stability of Sn0.75 to methyl orange, and (e,f) photocatalytic degradation of tetracycline solution and kinetic characteristic under Sn0.75.

negatively charged above this point. MO is anionic azo dye that exists as a quinoid structure under acidic conditions and an azo structure under basic conditions. Regardless of whether the solution is acidic or alkaline, methyl orange is anionic and negatively charged in an aqueous solution [33]. When the pH value of the solution is 7, the electrostatic attraction between the negatively charged MO and the weakly positively charged Sn0.75 surface results in slightly high adsorption [34].

In addition, the photocatalytic "memory" effect examinations of the samples were carried out after the samples were pre-illuminated for 1 h. The results are shown in Fig. 7. As can be seen from Fig. 7, the remove rate of MO solution added Cu-Cu$_2$O in darkness almost coincides with that of pre-illuminated Cu-Cu$_2$O, and the removal rate is only 0.45% within 180 min, which is attributed to the adsorption of Cu-Cu$_2$O. The results mean Cu-Cu$_2$O has no continuous catalytic performance when the illumination is turned off, which means Cu-Cu$_2$O has no photocatalytic "memory" effect.

The removal rates of MO solution added Sn0.75 without and with pre-illumination for 1 h are 97.3% and 80.1% after 180 min in dark, respectively. Therefore, the removal rate of MO solution in darkness is increased by 17.2% when Sn0.75 pre-illuminated for 1 h is used as a photocatalyst. The result indicates that there is still a certain catalytic activity after the light is turned off, which indicates Sn0.75 possesses photocatalytic "memory" effect. Compared with literature, Se nanorods and Ag/g-C$_3$N$_4$/V$_2$O$_5$ show photocatalytic "memory" effect, and the removal rates of methylene blue solution in dark are increased by 14% and 27% when Se nanorods and Ag/g-C$_3$N$_4$/V$_2$O$_5$ pre-illuminated are used as a photocatalyst, respectively [35,36].

3.6. Exploration of photocatalysis mechanism

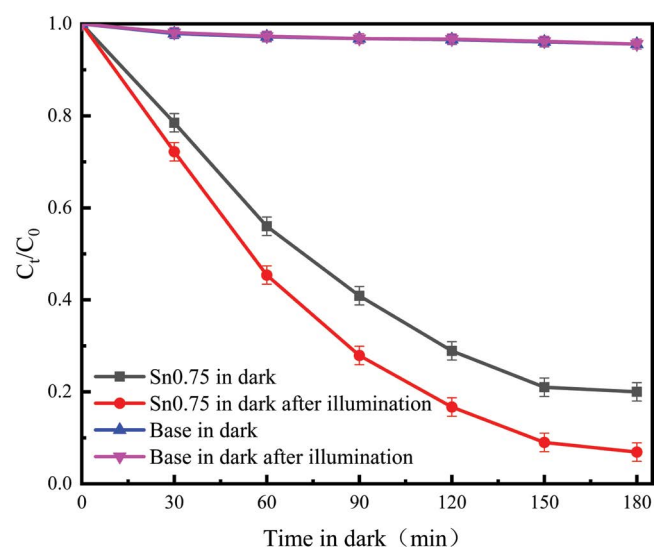To explore the possible mechanism, a series of radical quenching experiments were carried out to determine the activity types. Trapping agents of BQ, IPA and AO were used for superoxide anion radical ($^\bullet$O$_2^-$), hydroxyl radical ($^\bullet$OH) and hole (h$^+$), respectively. As shown in Fig. 8, the photodegradation efficiency of MO reached 93.7% under visible light irradiation, and the addition of BQ, IPA and AO reduces the photodegradation efficiency of MO to 60.2%, 50.8% and 3.4%, respectively. It is worth noting that the presence of $^\bullet$O$_2^-$, h$^+$ and $^\bullet$OH has a positive effect on the photocatalytic degradation of methyl orange. Among them, h$^+$ is the main active species, $^\bullet$O$_2^-$ and $^\bullet$OH are the secondary active species [37].

Cu$_2$O is a *p*-type semiconductor and SnO$_2$ is an n-type semiconductor in the Cu-Cu$_2$O/SnO$_2$ composite. Moreover, the conduct and valence bands of Cu$_2$O are both higher than that of SnO$_2$ [38,39]. The *p-n* heterojunctions of Cu$_2$O and SnO$_2$ could largely enhance the charge carrier separation. In addition, Cu is a good electron acceptor, which could facilitate the separation of electron–hole-pairs [40]. Therefore, the photocatalytic performance of the Cu-Cu$_2$O/SnO$_2$ samples are largely enhanced, compared with Cu$_2$O.

In order to reveal the carrier separation efficiency and transfer efficiency, the transient photocurrent response was performed. As shown in Fig. 9a, the photocurrent density of Sn0.75 is higher than that of Sn0, which means Sn0.75 could inhibit the carrier recombination effectively. The charge transfer efficiency was also evaluated by EIS, as shown in Fig. 9b. The result shows that Sn0.75 has a smaller arc radius, which indicates Sn0.75 has a higher charge separation efficiency than pure Sn0. The EIS result is consistent with the instantaneous photocurrent response result. Therefore, from the above findings, it can be concluded that the heterojunction of Cu-Cu$_2$O/SnO$_2$ promotes the separation and transfer of charge carriers as well as the photocatalytic activity [41].

A possible photocatalytic mechanism is proposed as shown in Fig. 10. When the solar energy absorbed by the sample is greater than its own bandgap energy, the electrons in the valence band (VB) of the sample are excited and then transfer to the conduction band (CB), while the holes remain in VB, thus forming electron–hole pairs. The h$^+$ produced

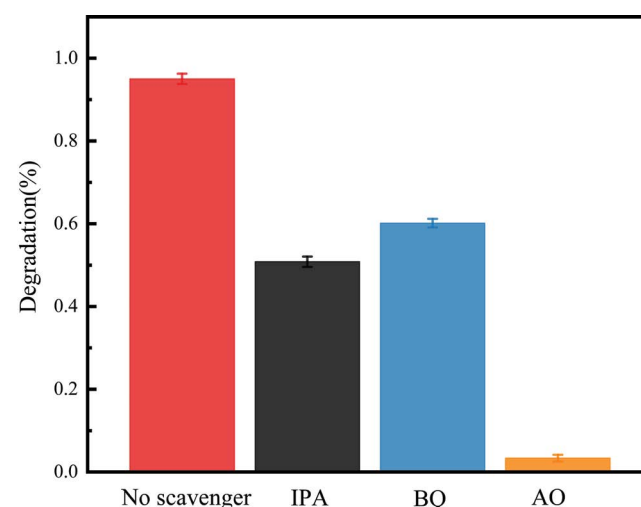Fig. 7. Removal of methyl orange by base and Sn0.75 in dark with and without pre-illumination.

Fig. 8. Methyl orange photodegradation under Sn0.75 with different radical trapping agents.
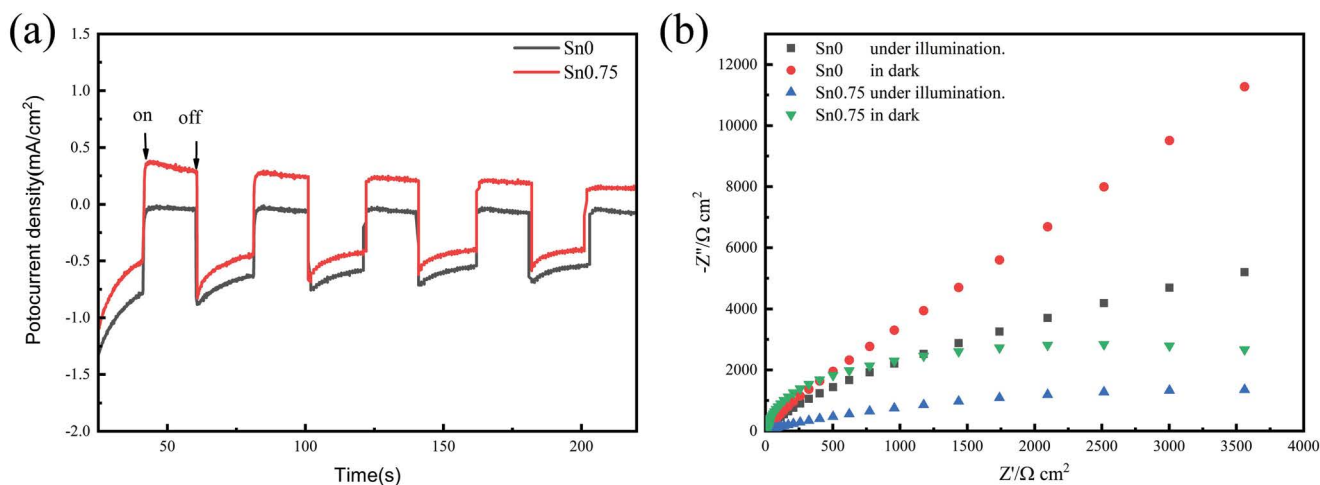
Fig. 9. (a) Transient photocurrent response curves and (b) electrochemical impedance spectroscopy spectra of the samples.
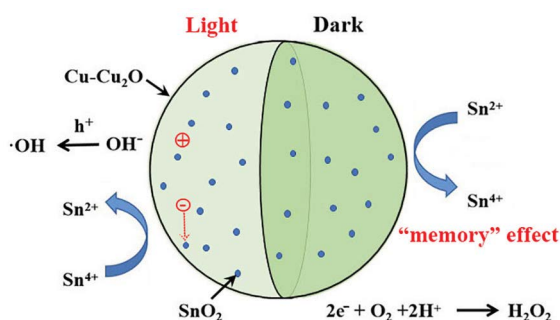

Fig. 10. Schematic diagram of charge migration mechanism of $Cu-Cu_2O/SnO_2$ nanocomposite.

will form hydroxyl radicals with OH^- in the water, and then REDOX reactions will occur with pollutants in the water. The electrons easily transfer from the conduction band of Cu_2O to that of SnO_2 [42], and are trapped and stored by SnO_2 which results in Sn^{2+} forming. When the light is turned off, the stored electrons are released from Sn^{2+} and could react with O_2 to form superoxidation ($^\bullet O_2^-$) or the $^\bullet O_2^-$ generated reacts with H_2O molecules to form H_2O_2 [43], which play a decisive role in photocatalytic oxidation in dark after the light is shut off. Therefore, Sn0.75 shows the photocatalytic "memory" effect.

4. Conclusion

In conclusion, the photocatalyst $Cu-Cu_2O/SnO_2$ was successfully prepared through a solvothermal method. The content of SnO_2 in the composite was adjusted by controlling the amount of Sn precursor. SnO_2 could effectively enhance the photocatalytic activity of $Cu-Cu_2O$ under visible light illumination. Furthermore, $Cu-Cu_2O/SnO_2$ photocatalyst shows the post-illumination "memory" activity in dark.

Acknowledgments

References

[1] C. Chen, H. Zeng, M. Yi, G. Xiao, S. Xu, S. Shen, B. Feng, *In-situ* growth of Ag_3PO_4 on calcined Zn-Al layered double hydroxides for enhanced photocatalytic degradation of tetracycline under simulated solar light irradiation and toxicity assessment, Appl. Catal., B, 252 (2019) 47–54.

[2] X.N. Hu, Y. Ye, W.B. Dong, Y.C. Huang, M.S. Zhu, Quantitative evaluation of structure-activity relationships in heterogeneous photocatalytic oxidation towards organic contaminants, Appl. Catal., B, 309 (2022) 121238, doi: 10.1016/j.apcatb.2022.121238.

[3] K. Domagala, C. Jacquin, M. Borlaf, B. Sinnet, T. Julian, D. Kata, T. Graule, Efficiency and stability evaluation of Cu_2O/MWCNTs filters for virus removal from water, Water Res., 179 (2020) 115879, doi: 10.1016/j.watres.2020.115879.

[4] D. Pathania, A. Sharma, S. Kumar, A.K. Srivastava, A. Kumar, L. Singh, Bio-synthesized Cu-ZnO hetro-nanostructure for catalytic degradation of organophosphate chlorpyrifos under solar illumination, Chemosphere, 277 (2021) 130315, doi: 10.1016/j.chemosphere.2021.130315.

[5] A. Kumar, G. Sharma, M. Thakur, D. Pathania, Sol-gel synthesis of polyacrylamide stannic arsenate nanocomposite ion exchanger: binary separations and enhanced photocatalytic activity, SN Appl. Sci., 1 (2019) 862, doi: 10.1007/s42452-019-0905-6.

[6] A. Kumar, D. Pathania, N. Gupta, P. Raj, A. Sharma, Photodegradation of noxious pollutants from water system using *Cornulaca monacantha* stem supported $ZnFe_2O_4$ magnetic bio-nanocomposite, Sustainable Chem. Pharm., 18 (2020) 100290, doi: 10.1016/j.scp.2020.100290.

[7] M. Liu, T. Peng, H. Li, L. Zhao, Y. Sang, Q. Feng, L. Xu, Y. Jiang, H. Liu, J. Zhang, Photoresponsive nanostructure assisted green synthesis of organics and polymers, Appl. Catal., B, 249 (2019) 172–210.

[8] N.A. Khan, S.H. Jhung, Adsorptive removal and separation of chemicals with metal–organic frameworks: contribution of pi-complexation, J. Hazard. Mater., 325 (2017) 198–213.

[9] K. Hemine, N. Lukasik, M. Gazda, I. Nowak, β-cyclodextrin-containing polymer based on renewable cellulose resources for effective removal of ionic and non-ionic toxic organic pollutants from water, J. Hazard. Mater., 418 (2021) 126286, doi: 10.1016/j.jhazmat.2021.126286.

[10] S. Singh, R. Punia, K.K. Pant, P. Biswas, Effect of work-function and morphology of heterostructure components on CO_2

reduction photo-catalytic activity of MoS$_2$-Cu$_2$O heterostructure, Chem. Eng. J., 433 (2022) 132709, doi: 10.1016/j.cej.2021.132709.

[11] J. Li, A.N. Pham, R. Dai, Z. Wang, T.D. Waite, Recent advances in Cu-Fenton systems for the treatment of industrial wastewaters: role of Cu complexes and Cu composites, J. Hazard. Mater., 392 (2020) 122261, doi: 10.1016/j.jhazmat.2020.122261.

[12] L.K. Cui, L.Q. Hu, Q.Q. Shen, X.G. Liu, H.S. Jia, J.B. Xue, Three-dimensional porous Cu$_2$O with dendrite for efficient photocatalytic reduction of CO$_2$ under visible light, Appl. Surf. Sci., 581 (2022) 152343, doi: 10.1016/j.apsusc.2021.152343.

[13] X.S. Zhou, B. Jin, J. Luo, X.X. Gu, S.Q. Zhang, Photoreduction preparation of Cu$_2$O@polydopamine nanospheres with enhanced photocatalytic activity under visible light irradiation, J. Solid State Chem., 254 (2017) 56–61.

[14] H.M. Zhu, Y. Li, X.C. Jiang, Room-temperature synthesis of cuprous oxide and its heterogeneous nanostructures for photocatalytic applications, J. Alloys Compd., 772 (2019) 447–459.

[15] J.F. Zhang, P. Wang, C.P. Yu, X. Shu, L. Jiang, Enhanced visible-light photoelectrochemical behavior of heterojunction composite with Cu$_2$O nanoparticles-decorated TiO$_2$ nanotube arrays, New J. Chem., 38 (2014) 4975–4984.

[16] J. Shravanti, J.I. Samuel, S.V. Manorama, Convenient architectures of Cu$_2$O/SnO$_2$ type II p-n heterojunctions and their application in visible light catalytic degradation of Rhodamine B, RSC. Adv., 6 (2016) 43672–43684.

[17] S.H. Liu, Y.S. Wei, J.S. Lu, Visible-light-driven photodegradation of sulfamethoxazole and methylene blue by Cu$_2$O/rGO photocatalysts, Chemosphere, 154 (2016) 118–123.

[18] S.W. Lee, J.W. Hong, H. Lee, D.H. Wi, S.M. Kim, S.W. Han, J.Y. Park, The surface plasmon-induced hot carrier effect on the catalytic activity of CO oxidation on a Cu$_2$O/hexoctahedral Au inverse catalyst, Nanoscale, 10 (2018) 10835–10843.

[19] Q. Li, Y.W. Li, P.G. Wu, R.C. Xie, Palladium oxide nanoparticles on nitrogen-doped titanium oxide: accelerated photocatalytic disinfection and post-illumination catalytic "memory", Adv. Mater., 20 (2008) 3717–3723.

[20] Q. Li, Y.W. Li, Z.Q. Liu, R.C. Xie, K.S. Jian, Memory antibacterial effect from photoelectron transfer between nanoparticles and visible light photocatalyst, J. Mater. Chem., 20 (2010) 1068–1072.

[21] L.N. Li, Z.S. Liu, L.T. Guo, H.L. Fan, X.Y. Tao, NaBiO$_3$/BiO$_{2-x}$ composite photocatalysts with post-illumination "memory" activity, Mater. Lett., 234 (2019) 30–34.

[22] M. Wei, C.S. Chen, X. Chen, X.Y. Liu, Z. Yang, F. Ding, Z.S. Chao, T.G. Liu, Low-temperature construction of MoS$_2$ quantum dots/ZnO spheres and their photocatalytic activity under natural sunlight, J. Colloid Interface Sci., 530 (2018) 714–724.

[23] T. Cai, Y.T. Liu, L.L. Wang, W.Y. Dong, G.M. Zeng, Recent advances in round-the-clock photocatalytic system: mechanisms, characterization techniques and applications, J. Photochem. Photobiol., C, 39 (2019) 58–75.

[24] W. Yang, Y. Chen, S. Gao, L.C. Sang, R.G. Tao, C.X. Sun, J.K. Shang, Q. Li, Post-illumination activity of Bi$_2$WO$_6$ in the dark from the photocatalytic "memory" effect, J. Adv. Ceram., 10 (2021) 355–367.

[25] M.Y. Kuo, C.F. Hsiao, Y.H. Chiu, T.H. Lai, Y.J. Hsu, Au@Cu$_2$O core@shell nanocrystals as dual-functional catalysts for sustainable environmental applications, Appl. Catal., B, 242 (2019) 499–506.

[26] S. Begum, S.R. Mishra, M. Ahmaruzzaman, Facile synthesis of NiO-SnO$_2$ nanocomposite for enhanced photocatalytic degradation of Bismarck brown, Inorg. Chem. Commun., 143 (2022) 109721, doi: 10.1016/j.inoche.2022.109721.

[27] S.M. Lam, Z.H. Jaffari, J.C. Sin, H.H. Zeng, H. Lin, H.X. Li, A.R. Mohamed, D.Q. Ng, Surface decorated coral-like magnetic BiFeO$_3$ with Au nanoparticles for effective sunlight photodegradation of 2,4-D and *E. coli* inactivation, J. Mol. Liq., 326 (2021) 115372, doi: 10.1016/j.molliq.2021.115372.

[28] B. Pan, Y. Wu, B. Rhimi, J. Qin, Y. Huang, M. Yuan, C. Wang, Oxygen-doping of ZnIn$_2$S$_4$ nanosheets towards boosted photocatalytic CO$_2$ reduction, J. Energy Chem., 57 (2021) 1–9.

[29] V. Kumar, V. Kumar, S. Som, J.H. Neethling, E. Olivier, O.M. Ntwaeaborwa, H.C. Swart, The role of surface and deep-level defects on the emission of tin oxide quantum dots, Nanotechnology, 25 (2014) 135701, doi: 10.1088/0957-4484/25/13/135701.

[30] J.F. Zhang, Y. Wang, T.K. Shen, X. Shu, J.W. Cui, Z. Chen, Y.C. Wu, Visible light photocatalytic performance of Cu$_2$O/TiO$_2$ nanotube heterostructures prepared by pulse deposition, Acta Phys. Chim. Sin., 30 (2014) 1535–1542.

[31] D.J. Yang, I. Kamienchick, D.Y. Youn, A. Rothschild, I.D. Kim, Ultrasensitive and highly selective gas sensors based on electrospun SnO$_2$ nanofibers modified by Pd loading, Adv. Funct. Mater., 20 (2010) 4258–4264.

[32] L.M. Liu, W.Z. Sun, W.Y. Yang, Q. Li, J.K. Shang, Post-illumination activity of SnO$_2$ nanoparticle-decorated Cu$_2$O nanocubes by H$_2$O$_2$ production in dark from photocatalytic "memory", Sci. Rep., 6 (2016) 20878, doi: 10.1038/srep20878.

[33] X.Z. Yang, C.Y. Wang, B. Zhou, S.C. Cheng, Characterization of an iron-copper bimetallic metal-organic framework for adsorption of methyl orange in aqueous solution, J. Autom. Methods Manage. Chem., 2023 (2023) 9985984, doi: 10.1155/2023/9985984.

[34] X.Y. Cheng, R.Q. Guan, Y.N. Chen, Y.D. Qian, Q.K. Shang, Y.N. Sun, Adsorption and photocatalytic degradation process of oxytetracycline using mesoporous Fe-TiO$_2$ based on high-resolution mass spectrometry, Chem. Eng. J., 460 (2023) 141618, doi: 10.1016/j.cej.2023.141618.

[35] H.S. El-Sheshtawy, H.M. El-Hosainy, K.R. Shoueir, I.M. El-Mehasseb, M. El-Kemary, Facile immobilization of Ag nanoparticles on g-C$_3$N$_4$/V$_2$O$_5$ surface for enhancement of post-illumination, catalytic, and photocatalytic activity removal of organic and inorganic pollutants, Appl. Surf. Sci., 467 (2019) 268–276.

[36] Y.D. Chiou, Y.J. Hsu, Room-temperature synthesis of single-crystalline Se nanorods with remarkable photocatalytic properties, Appl. Catal., B, 105 (2011) 211–219.

[37] Y. Jia, Y. Zhang, X. Zhang, J.H. Cheng, Y.J. Xie, Y. Zhang, X.Y. Yin, F. Song, H.Y. Cui, Novel CdS/PANI/MWCNTs photocatalysts for photocatalytic degradation of xanthate in wastewater, Sep. Purif. Technol., 309 (2023) 123022, doi: 10.1016/j.seppur.2022.123022.

[38] H. Gao, Y.W. Hu, Y. Xue, One-step solvothermal synthesis of Cu-Cu$_2$O composite with improved photocatalytic activity under visible light irradiation, Micro Nano Lett., 14 (2019) 1136–1139.

[39] J.W. Li, J.S. Guo, J.X. Zhang, Z.L. Sun, J.P. Gao, Surface etching and photodeposition nanostructures core-shell Cu$_2$O@CuO-Ag with S-scheme heterojunction for high efficiency photocatalysis, Surf. Interfaces, 34 (2022) 102308, doi: 10.1016/j.surfin.2022.102308.

[40] K. Daideche, H. Lahmar, D. Lerari, A. Azizi, Influence of deposition potential on the electrochemical growth and photocatalysis performance of SnO$_2$ nanostructures, Inorg. Chem. Commun., 147 (2023) 110154, doi: 10.1016/j.inoche.2022.110154.

[41] L. Zhao, S.M. Lam, Y.T. Ong, J.C. Sin, H.H. Zeng, Q.D. Xie, J.W. Lim, Fe$_2$WO$_6$ coupling on cube-like SrTiO$_3$ as a highly active S-scheme heterojunction composite for visible light photocatalysis and antibacterial applications, Environ. Technol. Innovation, 28 (2022) 102941, doi: 10.1016/j.eti.2022.102941.

[42] H.M. Zhang, W. Xu, G. Li, Z.M. Liu, Z.C. Wu, B.G. Li, Assembly of coupled redox fuel cells using copper as electron acceptors to generate power and its *in-situ* retrieval, Sci. Rep., 6 (2016) 21059, doi: 10.1038/srep21059.

[43] C.M. Fan, Y. Peng, Q. Zhu, L. Lin, R.X. Wang, A.W. Xu, Synproportionation reaction for the fabrication of Sn^{2+} self-doped SnO$_{2-x}$ nanocrystals with tunable band structure and highly efficient visible light photocatalytic activity, J. Phys. Chem. C, 46 (2013) 24157–24166.